AOGS
Acta Obstetricia et Gynecologica Scandinavica

AOGS ORIGINAL RESEARCH ARTICLE

Postpartum computed tomography angiography of the fetoplacental macrovasculature in normal pregnancies and in those complicated by fetal growth restriction

METTE Ø. THUNBO[1,2], MARIANNE SINDING[1], ANNE S. KORSAGER[2], JENS B. FRØKJÆR[3,4], LASSE R. ØSTERGAARD[2], ASTRID PETERSEN[5], CHARLOTTE OVERGAARD[2] & ANNE SØRENSEN[1,4]

[1]Department of Obstetrics and Gynecology, Aalborg University Hospital, Aalborg, [2]Department of Health Science and Technology, Aalborg University, Aalborg, [3]Department of Radiology, Aalborg University Hospital, Aalborg, [4]Department of Clinical Medicine, Aalborg University, Aalborg, and [5]Department of Pathology, Aalborg University Hospital, Aalborg, Denmark

Key words
Computed tomography angiography, fetal growth restriction, macrovasculature, placenta, vasculature

Correspondence
Anne Sørensen, Department of Obstetrics and Gynecology, Aalborg University Hospital, Reberbansgade 15, 9000 Aalborg, Denmark.
E-mail: annenoedgaard@hotmail.com

Conflict of interest
The authors have stated explicitly that there are no conflicts of interest in connection with this article.

Please cite this article as: Thunbo MØ, Sinding M, Korsager AS, Frøkjær JB, Østergaard LR, Petersen A, et al. Postpartum computed tomography angiography of the fetoplacental macrovasculature in normal pregnancies and in those complicated by fetal growth restriction. Acta Obstet Gynecol Scand 2018; 97:322–329.

Received: 28 July 2017
Accepted: 20 December 2017

DOI: 10.1111/aogs.13289

Abstract

Introduction. Current knowledge of the fetoplacental vasculature in fetal growth restriction (FGR) due to placental dysfunction focuses on the microvasculature rather than the macrovasculature. The aim of this study was to investigate the feasibility of computed tomography angiography to analyze the fetoplacental macrovasculature in normal and FGR pregnancies. *Material and methods.* We included 29 placentas (22–42 weeks of gestation) from normal birthweight pregnancies and eight placentas (26–37 weeks of gestation) from FGR pregnancies (birthweight < −15% and abnormal umbilical Doppler flow). We performed postpartum placental computed tomography angiography followed by semi-automatic three-dimensional image segmentation. *Results.* A median of nine (range seven to eleven) vessel generations was identified. In normal birthweight placentas, gestational age was positively linearly correlated with macrovascular volume ($p = 0.002$), vascular surface area ($p < 0.0005$) and number of vessel junctions ($p = 0.012$), but not with vessel diameter and inter-branch length. The FGR placentas had a lower weight ($p = 0.004$) and smaller convex volume ($p = 0.022$) (smallest convex volume containing the macrovasculature); however, macrovascular volume was not significantly reduced. Hence, macrovascular density given as macrovascular outcomes per placental volume was increased in FGR placentas: macrovascular volume per convex volume ($p = 0.004$), vascular surface area per convex volume ($p = 0.004$) and number of vessel junctions per convex volume ($p = 0.037$). *Conclusions.* Evaluation of the fetoplacental macrovasculature is feasible with computed tomography angiography. In normal birthweight placentas, macrovascular volume and surface area increase as pregnancy advances by vessel branching rather than increased vessel diameter and elongation. The FGR placenta was smaller; however, the macrovascular volume was within normal range because of an increased macrovascular density.

Abbreviations: 3D, three-dimensional; BW, birthweight; CTA, computed tomography angiography; FGR, fetal growth restriction; GA, gestational age; PVM, placental vascular malperfusion.

Introduction

Placental dysfunction leading to fetal growth restriction (FGR) complicates 3% of all pregnancies and is associated with adverse neonatal outcomes (1). The underlying cause of placental dysfunction is not completely understood, but maternal malperfusion leading to placental hypoxia and subsequent abnormal development of the fetoplacental vasculature is a possible etiology (2).

The human fetoplacental vasculature consists of the conductive part: chorionic vessels, stem villi vessels, intermediate villi vessels; and the functional unit: the terminal villi capillaries. Current knowledge on the fetoplacental vasculature in FGR pregnancies predominantly focuses on the microvasculature including the intermediate and terminal villi vessels. Several studies report a hypovascularized microvasculature of the FGR placenta with reduced vascular volume and surface area of the terminal villi capillaries due to fewer vessel branches and vessel elongation (3,4). In contrast, the fetoplacental macrovasculature, considered as the chorionic vessels and stem villi vessels, is only sparsely described. In the FGR placenta, the total macrovascular volume is reduced (5). However, conflicting evidence exists regarding the macrovascular branching pattern of the FGR placenta, as some studies indicate an abnormal pattern with magistral branching (6), a reduced number of stem villi vessels (7), and discrepancies in vessel length density (8), whereas others demonstrate a normal macrovascular branching pattern (9,10).

Further knowledge of the fetoplacental macrovasculature may improve our understanding of the placental pathology associated with FGR. Imaging technologies such as computed tomography angiography (CTA) (11) and magnetic resonance angiography (11–13) provide new insights into the entire fetoplacental vasculature. Therefore, the aim of this study was to explore the feasibility of postpartum placental CTA with subsequent automatic three-dimensional (3D) image segmentation as a method for analyzing the fetoplacental macrovasculature in normal and FGR pregnancies.

Material and methods

We included 29 placentas at 22–42 weeks of gestation from singleton pregnancies with normal birthweight (BW) $\geq -15\%$ (Z-score ≥ -1.28) (14), and eight placentas at 26–37 weeks of gestation from singleton pregnancies complicated by FGR defined as BW $< -15\%$ and abnormal umbilical Doppler flow (Pulsatility index Z-score > 2) (15). All placentas were collected at Aalborg University Hospital, Denmark, between 1 July 2015 and 1 June 2016. Maternal and pregnancy characteristics of the included placentas are presented in Table 1. Clinical data were collected from medical records and the electronic ultrasound database ASTRAIA version 1.24.7 (Astraia Software GmbH, Munich, Germany).

Immediately after delivery, the placenta was stored in a freezer at −5°C. On the day of CTA, the placenta was thawed and photographed on a scale bar (Figure 1a, d). The umbilical vessels were cannulated 5 cm from the umbilical cord insertion and flushed with a saline 9 mg NaCl/mL and Heparin 4.5 IE/mL (Leo Pharma A/S, Ballerup, Denmark) solution until the venous efflux was clear. A heated (< 40°C) contrast mixture of gelatin 0.05 g/mL (Urtegaarden Djursland, Allingåbro, Denmark), barium sulfate 0.17 g/mL (E-Z Em Inc., Westbury, NY, USA), and saline 9 mg NaCl/mL was then injected with a hand syringe. When the contrast mixture appeared in the venous efflux, the vein was plugged, and injection was continued until resistance was felt. Hereafter the placenta was cooled (5°C) to set the gelatin solution. The placental preparation is a modified version of the preparation in the study by Langheinrich et al. (16,17).

CTA was performed using a 128-slice Siemens SOMATOM Definition Flash scanner (Siemens Healthcare GmbH, Erlangen, Germany) with software version VA48A within 2 h after preparation. The scanning parameters included 0.6-mm slice thickness, increment of 0.4 mm, a pitch of 1°, 140 kV, effective 200 mAs and a rotation time of 1 sec. DICOM data were exported to AW Server version 3.0 (GE Healthcare, Little Chalfont, UK) for 3D reconstruction of the fetoplacental macrovasculature (Figure 1b, e).

In an in-house program written in MATLAB (The Mathworks Inc., Natick, MA, USA), tubular structures were enhanced with a multi-scale vessel enhancement filtering method (18,19). On the filtered images, vessel segmentation was applied with an initial segmentation using the clustering method Fuzzy c-means, and hereafter a graph cut segmentation was performed (20,21). An automatic post-processing step confirmed that only connected vessel structures were included. Lastly, a skeleton (center line) of the vessels was computed (22) (Figure 1c, f). All

Key Message

Placental computed tomography angiography provides new insights into the fetoplacental macrovasculature. In normal pregnancy, macrovascular volume increases by vessel branching rather than vessel elongation. The fetal growth restriction placenta is smaller; however, the macrovascular volume is maintained because of an increased vascular density.

Characteristics	Normal BW group	FGR group	*p*-value
Maternal age, years	30.0 (4.6)	28.3 (6.0)	0.387
Maternal smoking, %	14.3 (4/28)	0.0 (0/8)	0.230
Maternal body mass index, kg/m^2	25.6 (5.1)	27.5 (6.9)	0.391
Nullipara, %	50.0 (14/28)	50.0 (4/8)	1.000
Pre-eclampsia[a], %	0.0 (0/28)	37.5 (3/8)	0.008
Gestational age, weeks	37.6 (33.1–40.5)	34.6 (26.8–36.7)	0.077[b]
Birthweight, Z-score	0.00 (−0.56 to 0.47)	−2.21 (0.37)	<0.0005[b]
Placental weight[c], Z-score	0.00 (0.98)	−1.25 (1.11)	0.004
Umbilical artery Doppler, Z-score	−0.06 (0.88)	3.13 (0.84)	<0.0005
Missing	6	0	
Cerebro-placental ratio Doppler, Z-score	0.12 (1.13)	−3.36 (0.81)	<0.005
Missing	22	0	

Data are given as mean (SD), median (interquartile range) or % (*n*/*N*).
[a]Diagnostic criteria: Preeclampsia (hypertension (systolic blood pressure > 140 mmHg and/or diastolic blood pressure > 100 mmHg) and proteinuria (0.3 g/24 h) or severe preeclampsia (diastolic blood pressure > 110 mmHg and/or subjective symptoms and abnormal blood samples).
[b]Comparison is based on Mann–Whitney *U*-test.
[c]Unfixed placenta weight.

Table 1. Maternal and pregnancy characteristics in normal birthweight (BW) group (n = 28) and fetal growth restriction (FGR) group (n = 8).

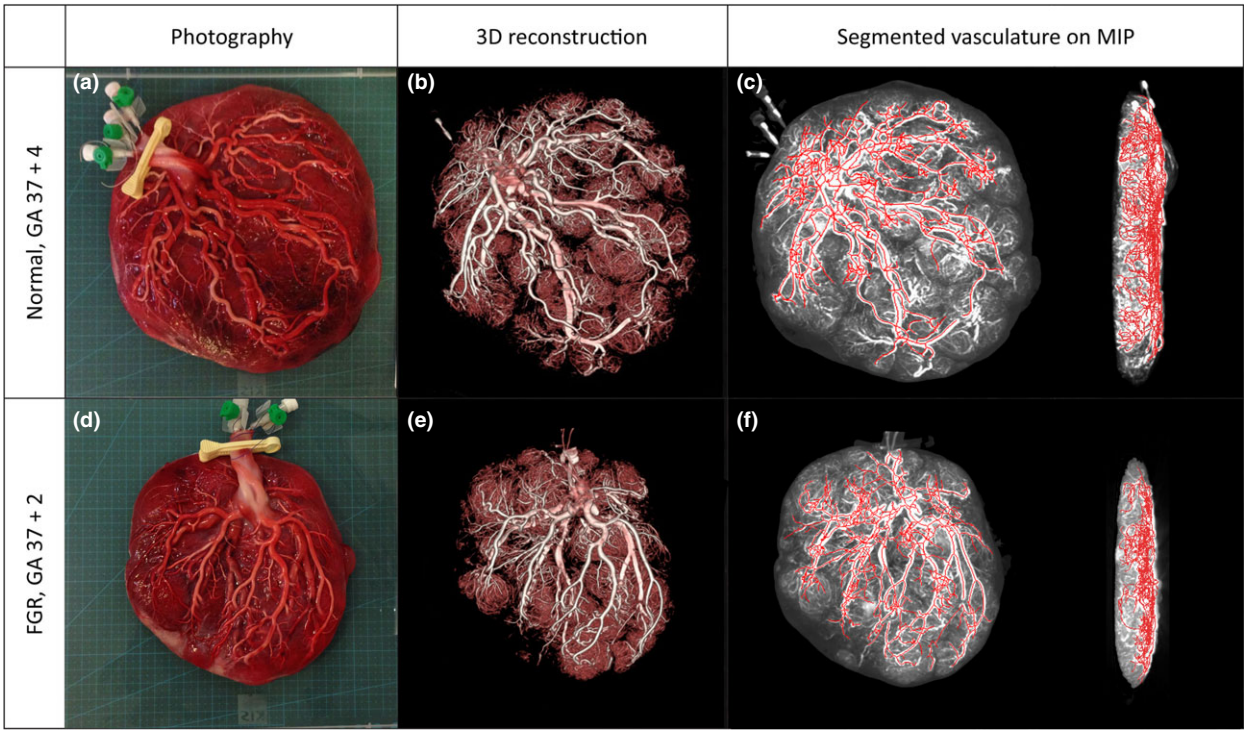

Figure 1. Images of a normal birthweight placenta (a, b and c) and a gestational-age-matched fetal growth restriction (FGR) placenta (d, e and f). Macroscopic photography (a and d), three-dimensional reconstructions of the major fetoplacental blood vessels (b and e) and the skeleton (center line) of the blood vessels obtained from the semi-automatic three-dimensional image segmentation layered on a maximum intensity projection (MIP) image (c and f). GA, gestational age. [Color figure can be viewed at wileyonlinelibrary.com].

segmentations were visually controlled. Only one normal BW placenta was excluded from further analysis due to the presence of extravascular contrast seen on placental 3D reconstruction. A manual correction was added to the segmentation in 42% (15/36) of the angiographies. Based on the 3D vessel segmentation the following

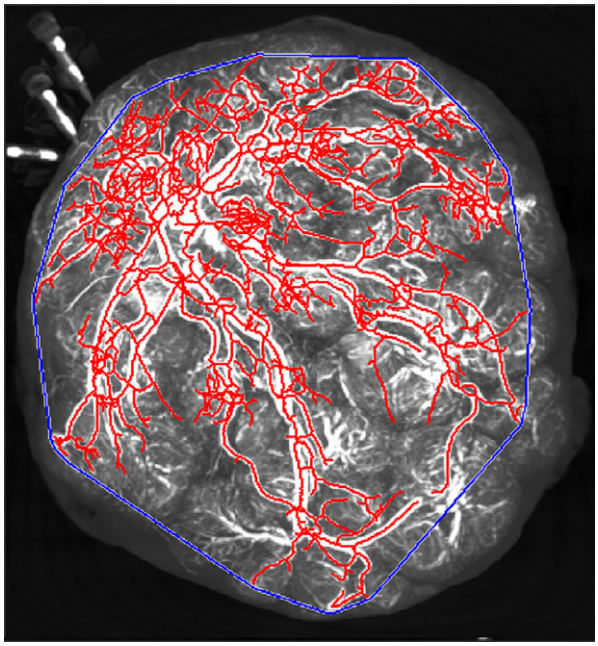

Figure 2. Illustration of the vascular outcome convex volume (mL) (blue line) on a maximum intensity projection image with skeleton line of the segmented vessels (red lines). [Color figure can be viewed at wileyonlinelibrary.com].

macrovascular outcomes were extracted: vascular volume, surface area, mean vessel diameter, number of vessel junctions, mean inter-branch length and size of the segmented fetoplacental macrovasculature (estimated as convex volume representing the smallest convex volume that contains the macrovasculature) (Figure 2).

In all placentas a pathological macro- and microscopic examination was performed according to a standard protocol (23) by an experienced placental pathologist (AP), who was blinded to the CTA macrovascular outcomes but not the clinical information. Only abnormal findings such as abnormal umbilical cord and signs of placental vascular malperfusion (PVM) defined as signs of maternal and/or fetal vascular malperfusion (23) were reported in this study.

In normal BW placentas, the relation between the macrovascular outcomes and gestational age (GA) was estimated using linear regression. Standardized variables (Z-scores) of the macrovascular outcomes were calculated based on the normal BW placentas. The macrovascular outcomes were compared between groups using the mean or median Z-scores to adjust for GA and independent Student's *t*-test or Mann–Whitney *U*-test. Differences were considered significant if $p < 0.05$. Analyses were performed in SPSS Statistics version 23.0 (IBM, North Castle, NY, USA).

Table 2. Correlation between gestational age and macrovascular outcomes extracted with three-dimensional image segmentation in normal birthweight placentas ($n = 28$).

Macrovascular outcome	*r*	*p*-value
Macrovascular volume (mL)	0.566	0.002
Surface area (mm^2)	0.631	<0.0005
Mean vessel diameter (mm)	0.209	0.285
Number of vessel junctions	0.466	0.012
Mean inter-branch length (mm)	0.016	0.936
Convex volume (mL)[a]	0.787	<0.0005

[a]Size of segmented fetoplacental macrovasculature.

Ethical approval

The study was approved by the Danish National Ethics Committee (N-20150018) and declared to the Danish Data Protection Agency (2008-58-0028). Written informed consent was obtained from all participants.

Results

With CTA and subsequent semi-automatic 3D image segmentation a median of nine (range seven to eleven) generations of fetoplacental blood vessels was visualized in normal BW placentas as well as in FGR placentas. As demonstrated by the side views, the segmentation includes the chorionic vessels on the fetal side of the placental surface and proceeds into the stem villi vessels perpendicular to the placental surface (Figure 1c, f).

In normal BW placentas, a positive linear correlation was demonstrated between GA and convex volume ($r = 0.787$, $p < 0.0005$), macrovascular volume ($r = 0.556$, $p = 0.002$), surface area ($r = 0.631$, $p < 0.0005$), and number of vessel junctions ($r = 0.466$, $p = 0.012$). In gestational week 30 the macrovascular volume was 15.5 mL and in gestational week 40 it was 26.7 mL. No correlation was found between GA and mean vessel diameter and mean inter-branch length (Table 2 and Figure 3).

The FGR placental weight was reduced ($p = 0.004$) and the convex volume containing the macrovasculature was smaller ($p = 0.022$) when compared with the normal placenta at equivalent GA; however, the macrovascular volume was not significantly reduced ($p = 1.000$). In the FGR placentas, the macrovascular density, given as the vascular outcome per convex volume, was significantly increased when compared with the normal placenta at equivalent GA; macrovascular volume per convex volume ($p = 0.004$), surface area per convex volume ($p = 0.004$) and number of vessel junctions per convex volume ($p = 0.037$). Data are presented in Table 3 and Figure 3.

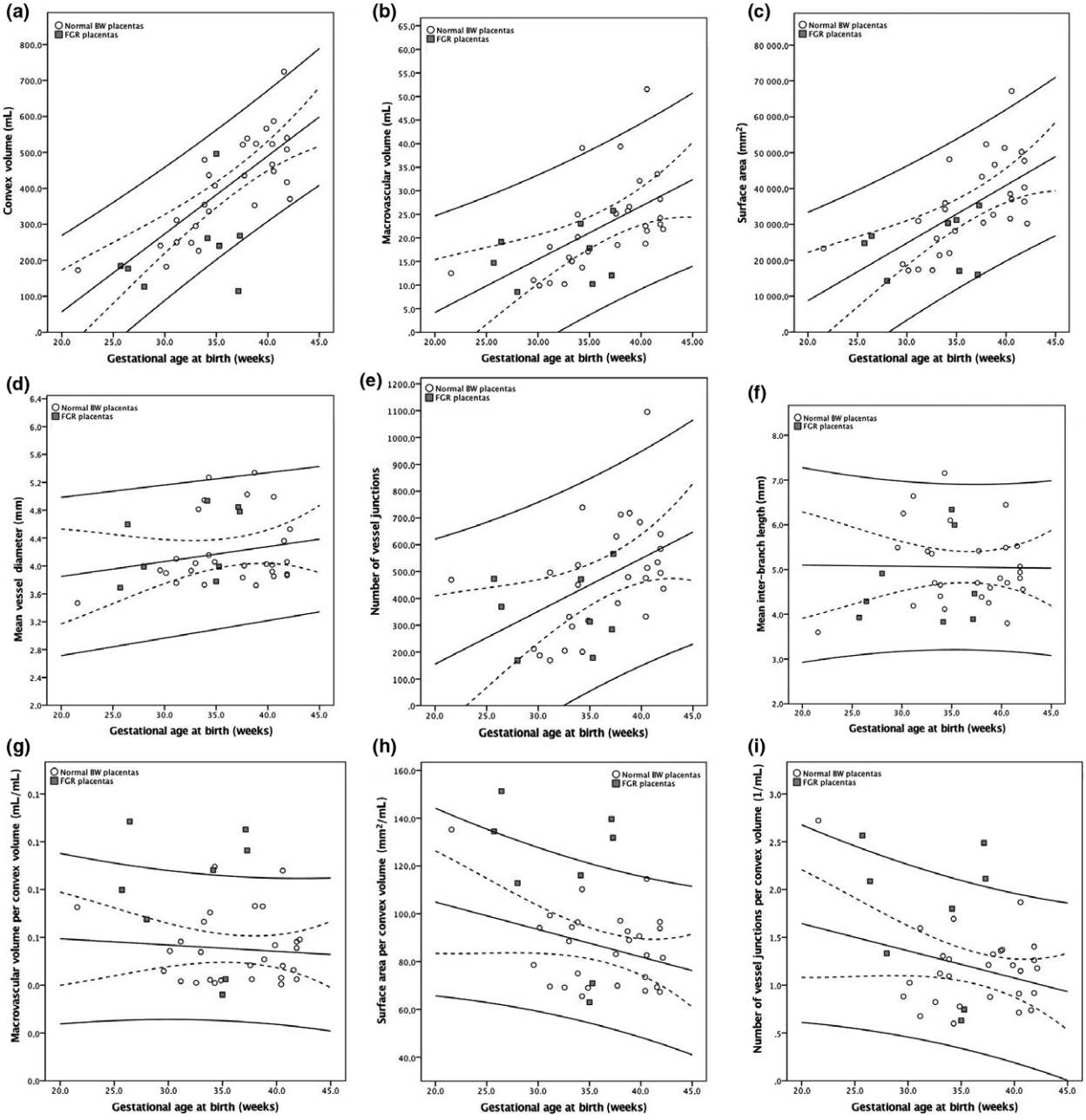

Figure 3. Associations between gestational age and (a) convex volume, (b) vascular volume, (c) surface area, (d) mean vessel diameter, (e) number of vessel junctions, (f) mean inter-branch length, (g) vascular volume per convex volume, (h) surface area per convex volume, and (i) number of vessel junctions per convex volume in normal birthweight placentas (circles). The solid lines indicate ordinary least squares fit and 95% PI. The dashed lines indicate 95% CI. The squares represent the fetal growth restriction (FGR) placentas.

The major placental pathological findings are presented in Table 4. Seven out of eight FGR placentas and seven out of 28 normal BW placentas exhibited signs of PVM. Placentas with major placental pathological findings are characterized in the Supplementary material (Table S1).

Discussion

This study demonstrates that analysis of the fetoplacental macrovasculature is feasible with CTA and subsequent semi-automatic 3D image segmentation. Our data indicate that in normal BW placentas, the macrovascular

Table 3. Fetoplacental macrovascular outcomes: fetal growth restriction (FGR) placentas (n = 8) compared with normal birthweight (BW) placentas (n = 28).

Macrovascular outcome	FGR group	p-value
Macrovascular volume, Z-score	−0.21 (0.86)	1.000[a]
Surface area, Z-score	−0.42 (1.00)	0.695[a]
Mean vessel diameter, Z-score	−0.42 (0.95)	0.358[a]
Number of vessel junctions, Z-score	−0.24 (0.89)	0.537[a]
Mean inter-branch length, Z-score	−0.41 (1.11)	0.320
Convex volume[b], Z-score	−1.06 (1.49)	0.022
Macrovascular volume per convex volume, Z-score	1.51 (1.88)	0.004
Surface area per convex volume, Z-score	1.52 (1.92)	0.004
Number of vessel junctions per convex volume, Z-score	1.02 (1.73)	0.037

Data are given as mean (SD).
[a]Comparison is based on Mann–Whitney *U*-test.
[b]Size of segmented fetoplacental macrovasculature.

Table 4. Major placental abnormalities[a] in normal birthweight (BW) placentas (n = 28) and fetal growth restriction (FGR) placentas (n = 9).

Pathological characteristics[a]	Normal BW placentas % (*n*/*N*)	FGR placentas% (*n*/*N*)
Placental vascular malperfusion	25.0 (7/28)	88.9 (8/9)
Maternal vascular malperfusion	7.0 (2/28)	55.6 (5/9)
Fetal vascular malperfusion	18.0 (5/28)	22.2 (2/9)
Maternal and fetal vascular malperfusion	0.0 (0/28)	11.1 (1/9)
Marginal umbilical cord insertion (< 1 cm from the nearest margin)	11.0 (3/28)	0.0 (0/9)
Hypocoiled umbilical cord (< 1 coil per 10 cm)	10.7 (3/28)	0.0 (0/9)

[a]Categorization based on Khong et al. 2016 (23).

volume and surface area increase during pregnancy due to vessel branching rather than increased vessel diameter and vessel elongation. The FGR placenta is smaller when compared with the normal BW placenta at equivalent GA; however surprisingly, the total macrovascular volume is not significantly reduced. In the FGR placenta, the macrovascular volume remains within the normal range in spite of a smaller placental size because of an increased macrovascular density.

Our study had some methodological limitations. Some underestimation of the segmented macrovascular volume may have been present due to intravascular blood clots. In this study, the placentas were frozen postpartum and flushed with heparinized saline – both are known to reduce blood clotting (24). Following the automatic 3D image segmentation, a manual segmentation was added to correct for any under-segmentation. In this study, we visualized up to 11 generations of the fetoplacental blood vessels including chorionic and stem villi vessels. Previous studies on placental magnetic resonance angiography (12,13) and placental CTA and magnetic resonance angiography (11) have demonstrated four (12) to six (11) generations of fetoplacental blood vessels. The improvement of vessel visualization of our study might rely on the specific preparation of the placenta and the semi-automatic 3D image segmentation.

The strength of this method is the demonstration of the entire fetoplacental macrovasculature, which is an advantage when compared with studies based on placental biopsies (7,10). The placenta is a heterogeneously structured organ, and the vascular pathology might be unevenly distributed within it. In addition, 3D imaging provides information on spatial vessel architecture including vessel surface area and vessel branching pattern, which is not available by conventional two-dimensional imaging (25). Another strength of CTA is that it allows subsequent placental pathological examination, which is not available following corrosion casts. Furthermore, the semi-automatic 3D image segmentation enables an objective and quantitative vascular analysis.

Another strength of this study is the placental pathological examination to confirm that low BW pregnancies are caused by placental dysfunction. The majority of the FGR cases (seven out of eight, 86%) demonstrated pathological signs of PVM. Placental examination also revealed signs of PVM in seven out of 28 normal BW placentas (25%). These findings are in accordance with a previous study demonstrating PVM in a small proportion of normal pregnancies and normal placental examination in a small proportion of FGR pregnancies (26). Another strength was adjusting for GA in the data analysis. This is important, because the placental vasculature changes dramatically as pregnancy advances (27). A limitation of the study design is the small number of normal BW placentas especially from early GA and the number of FGR placentas. Yet the strict inclusion criteria were set to select FGR cases caused by placental dysfunction and not just constitutionally small cases.

In the normal BW placentas, we found that the fetoplacental macrovascular volume and surface area increase linearly with GA, and our data indicated that vessel branching rather than increasing vessel diameter or vessel elongations dominate this macrovascular growth. These findings are in contrast to previous reviews reporting that stem villi vessel growth in normal pregnancies is characterized by branching angiogenesis until mid-gestation, followed by non-branching angiogenesis in the third trimester (28). This difference may be explained by the

analysis of the entire fetoplacental macrovasculature (chorionic vessels as well as stem villi vessels) in this current study.

In this study the macrovascular volume was 15.5 mL in gestational week 30 and 26.7 mL in gestational week 40. Based on previous literature, the extra-fetal vascular volume should account for approximately one-third of the total fetal vascular volume (29), which is known to be far more than the volume estimated by CTA in this study. Our findings suggest that the peripheral placental microvasculature, which is not segmented by this method, contains a considerable amount of the fetal blood. In addition, fetal blood contained in the umbilical cord may also have contributed to this difference.

When comparing normal BW and FGR placentas at equivalent GA, we demonstrated that the weight of the FGR placenta was reduced. This finding is in accordance with previous FGR studies (30). However, surprisingly we found that in the FGR placenta the fetoplacental macrovascular volume did not differ significantly from that in normal BW placentas. This finding may be in contrast to a previous study on corrosion casting by Gong et al. (5) reporting significantly reduced fetoplacental vascular volume in FGR placentas. In that study, however, the fetoplacental vascular volume was estimated as the total volume of perfusate needed to fill the total fetoplacental vasculature. Hence, both the fetoplacental micro- and macrovasculature was analyzed, which may explain the opposing results. According to our data, the macrovascular volume of the small FGR placenta remained within normal range because of an increased macrovascular density. The increased vascular density is in contrast with previous studies based on stereological and histological analysis of placental biopsies demonstrating that FGR placentas have a reduced length of stem villi vessels per length of villi in preterm FGR (10) or a reduced number of stem villi arteries per microscopic field (7). One explanation of the opposing findings could be that our study is based on CTA with 3D image segmentation of the entire macrovasculature including the chorionic vessels rather than placental biopsies.

Several studies suggest that the placental pathology associated with early- and late-onset FGR (31) may differ. Because of the small number of FGR cases included in this study, we did not perform any subgroup analysis. However, future studies in placental CTA may be able to demonstrate important vascular differences between the two FGR types.

In conclusion, investigation of the fetoplacental macrovasculature is feasible with CTA and subsequent 3D image segmentation. Important characteristics were revealed regarding the normal fetoplacental macrovascular development. By using postpartum placental CTA we found that the FGR placenta was smaller; however, the macrovascular blood volume remained within normal range because of an increased macrovascular density. Our study underlines CTA as a promising research method to analyze the fetoplacental macrovasculature.

Acknowledgments

We are grateful to Anne Staub Rasmussen, MD, for fruitful discussions regarding the angiography method and the placental preparation. The authors thank Pernille Veiss-Pedersen, radiographer, for competent assistance in performing the CTA.

Funding

This work was supported by The Faculty of Medicine at Aalborg University and by Aalborg University Hospital in The North Denmark Region.

References

1. Cosmi E, Fanelli T, Visentin S, Trevisanuto D, Zanardo V, Cosmi E, et al. Consequences in infants that were intrauterine growth restricted. J Pregnancy. 2011;2011:364381.
2. Kingdom JC, Kaufmann P. Oxygen and placental vascular development. Adv Exp Med Biol. 1999;474:259–75.
3. Kuzmina IY, Hubina-Vakulik GI, Burton GJ. Placental morphometry and Doppler flow velocimetry in cases of chronic human fetal hypoxia. Eur J Obstet Gynecol Reprod Biol. 2005;120:139–45.
4. Todros T, Sciarrone A, Piccoli E, Guiot C, Kaufmann P, Kingdom J. Umbilical Doppler waveforms and placental villous angiogenesis in pregnancies complicated by fetal growth restriction. Obstet Gynecol. 1999;93:499–503.
5. Gong SP, Zhao YT, Yu YH. Vascular network modeling reveals significant differences in vascular morphology in growth-restricted placentas. Rev Obstet Gynecol. 2011;4:103–8.
6. Nordenvall M, Ullberg U, Laurin J, Lingman G, Sandstedt B, Ulmsten U. Placental morphology in relation to umbilical artery blood velocity waveforms. Eur J Obstet Gynecol Reprod Biol. 1991;40:179–90.
7. Almasry SM, Eldomiaty MA, Elfayomy AK, Habib FA, Safwat MD. Structural analysis of human placental stem and terminal villi from normal and idiopathic growth restricted pregnancies. J Mol Histol. 2012;43:263–71.
8. Junaid TO, Bradley RS, Lewis RM, Aplin JD, Johnstone ED. Whole organ vascular casting and microCT examination of the human placental vascular tree reveals novel alterations associated with pregnancy disease. Sci Rep. 2017;7:4144.

9. Junaid TO, Brownbill P, Chalmers N, Johnstone ED, Aplin JD. Fetoplacental vascular alterations associated with fetal growth restriction. Placenta. 2014;35:808–15.
10. Jackson MR, Walsh AJ, Morrow RJ, Mullen JB, Lye SJ, Ritchie JW. Reduced placental villous tree elaboration in small-for-gestational-age pregnancies: relationship with umbilical artery Doppler waveforms. Am J Obstet Gynecol. 1995;172:518–25.
11. Rasmussen AS, Lauridsen H, Laustsen C, Jensen BG, Pedersen SF, Uhrenholt L, et al. High-resolution ex vivo magnetic resonance angiography: a feasibility study on biological and medical tissues. BMC Physiol. 2010;10:3.
12. Wang ZJ, Zhu XW, Huang QT, Yun ZQ, Cao YW, Chen YY, et al. Three-dimensional reconstruction of human placental vascular network using in vitro MRI data. Ultrasound Obstet Gynecol. 2016;47:790–2.
13. Rasmussen AS, Stæhr-Hansen E, Lauridsen H, Uldbjerg N, Pedersen M. MR angiography demonstrates a positive correlation between placental blood vessel volume and fetal size. Arch Gynecol Obstet. 2014;290:1127–31.
14. Marsál K, Persson PH, Larsen T, Lilja H, Selbing A, Sultan B. Intrauterine growth curves based on ultrasonically estimated foetal weights. Acta Paediatr. 1996;85:843–8.
15. Parra-Cordero M, Lees C, Missfelder-Lobos H, Seed P, Harris C. Fetal arterial and venous Doppler pulsatility index and time averaged velocity ranges. Prenat Diagn. 2007;27:1251–7.
16. Langheinrich AC, Wienhard J, Vormann S, Hau B, Bohle RM, Zygmunt M. Analysis of the fetal placental vascular tree by X-ray micro-computed tomography. Placenta. 2004;25:95–100.
17. Langheinrich AC, Vorman S, Seidenstücker J, Kampschulte M, Bohle RM, Wienhard J, et al. Quantitative 3D micro-CT imaging of the human feto-placental vasculature in intrauterine growth restriction. Placenta. 2008;29:937–41.
18. Frangi AF, Niessen WJ, Vincken KL, Viergever MA. Multiscale vessel enhancement filtering. Lect Notes Comput Sci. 1998;1496:130–7.
19. Kroon D-J. Hessian based Frangi Vesselness filter [Internet]. 1999. Available online at: https://www.mathworks.com/matlabcentral/fileexchange/24409-hessian-based-frangi-vesselness-filter (accessed July 1, 2016).
20. Boykov Y, Kolmogorov V. An experimental comparison of min-cut/max-flow algorithms for energy minimization in vision. IEEE Trans Pattern Anal Mach Intell. 2004;26:1124–37.
21. Maier O. Graph-cut (max-flow/min-cut) [Internet]. 2014. Available online at: http://pythonhosted.org/MedPy/graphcut.html (accessed July 1, 2016).
22. Malandain G, Bertrand G, Ayache N. Topological segmentation of discrete surfaces. Int J Comput Vis. 1993;10:183–97.
23. Khong TY, Mooney EE, Ariel I, Balmus NCM, Boyd TK, Brundler M-A, et al. Sampling and definitions of placental lesions: Amsterdam Placental Workshop Group Consensus Statement. Arch Pathol Lab Med. 2016;140:698–713.
24. Cooper IS, Samra K, Wisniewska K. Effects of freezing on major arteries. Stroke. 1971;2:471–82.
25. Mayhew TM. Stereology and the placenta: where's the point? A review Placenta. 2006;27(Suppl A):17–25.
26. Pathak S, Lees CC, Hackett G, Jessop F, Sebire NJ. Frequency and clinical significance of placental histological lesions in an unselected population at or near term. Virchows Arch. 2011;459:565–72.
27. Benirschke K, Burton GJ, Baergen RN. Architecture of normal villous trees. Pathology of the Human Placenta. 6th edn. Berlin, Heidelberg: Springer-Verlag; 2012. pp. 101.
28. Mayhew T. A stereological perspective on placental morphology in normal and complicated pregnancies. J Anat. 2009;215:77–90.
29. Polin RA, Yoder MC. Workbook in Practical Neonatology, 5th edn. Amsterdam: Elsevier, 2015. p. 392.
30. Biswas S, Ghosh S. Gross morphological changes of placentas associated with intrauterine growth restriction of fetuses: a case control study. Early Hum Dev. 2008;84:357–62.
31. Mifsud W, Sebire NJ. Placental pathology in early-onset and late-onset fetal growth restriction. Fetal Diagn Ther. 2014;36:117–28.

Supporting information

Additional Supporting Information may be found in the online version of this article:

Table S1. Characteristics of placentas with major placental abnormalities.